Preparing and Analyzing Solitons in the Sine-Gordon Model with Quantum Gas Microscopes

Elisabeth Wybo,[1,2,*] Alvise Bastianello,[1,2] Monika Aidelsburger,[2,3] Immanuel Bloch,[2,3,4] and Michael Knap[1,2]

[1] *Technical University of Munich, TUM School of Natural Sciences, Physics Department, Garching 85748, Germany*

[2] *Munich Center for Quantum Science and Technology (MCQST), Schellingstrasse 4, München 80799, Germany*

[3] *Fakultät für Physik, Ludwig-Maximilians-Universität, Munich 80799, Germany*

[4] *Max-Planck-Institut für Quantenoptik, Garching 85748, Germany*

(Received 5 April 2023; revised 8 June 2023; accepted 22 June 2023; published 19 July 2023)

The sine-Gordon model emerges as a low-energy theory in a plethora of quantum many-body systems. Here, we theoretically investigate tunnel-coupled Bose-Hubbard chains with strong repulsive interactions as a realization of the sine-Gordon model deep in the quantum regime. We propose protocols for quantum gas microscopes of ultracold atoms to prepare and analyze solitons, which are the fundamental topological excitations of the emergent sine-Gordon theory. With numerical simulations based on matrix product states, we characterize the preparation and detection protocols and discuss the experimental requirements.

DOI: 10.1103/PRXQuantum.4.030308

I. INTRODUCTION

Universality forms one of the pillars for the classification of quantum phases of matter. Upon coarse graining, microscopic details become irrelevant and only symmetry and topology determine the essential properties. Seemingly different-looking microscopic systems can then be described by the same set of collective degrees of freedom that are captured by the same emergent effective field theory. A prominent example is the relativistic sine-Gordon field theory [1,2], which emerges as the low-energy description of various physical systems—including, among others, the massive Thirring model [1,3], the Coulomb gas [4], spin chain [5–7], bosonic and fermionic Hubbard models [8,9], and circuit quantum electrodynamics [10,11]—and thus is of central interest for a multifaceted community.

In the strongly interacting regime, the sine-Gordon model possesses a complex quasiparticle spectrum, consisting of solitons, which are massive topological excitations, and breathers, which are bound states of these solitons. Furthermore, the sine-Gordon model is a renowned example of an integrable field theory [12,13], which implies infinitely long-lived quasiparticles, unconventional relaxation dynamics [14], and unconventional transport [15,16]. Elegant analytical methods can be used to obtain exact results that have improved our understanding of the model [12,13,17–23]. Despite these advances from integrability, analytical predictions for correlation functions and the full-counting statistics of many observables, both in equilibrium and out of equilibrium, are very difficult to access. Moreover, it is pertinent to understand in which dynamical regimes the effective sine-Gordon field theory is realized in one of the microsocopic models described above [24]. This can lead to the development of highly tunable sine-Gordon quantum simulators, that are, for instance, based on ultracold atoms in optical lattices, Rydberg atoms, or trapped ions.

Pioneering theoretical work [25,26] has motivated the experimental realization of the sine-Gordon model with tunnel-coupled one-dimensional (1D) quasicondensates [27–29]. In these atom-chip implementations, the sine-Gordon mass scale can be tuned and correlation functions can be efficiently characterized by matter-wave interferometry [27,30–34] but the interactions in the 1D gases have been restricted to being rather weak. As a consequence, the emergent sine-Gordon field theory is approximately semiclassical [27,35,36]. From this perspective, tunnel-coupled optical-lattice systems can be very convenient: they allow the kinetic energy to be quenched and, hence, the effective interactions to be enhanced. Although,

*elisabeth.wybo@tum.de

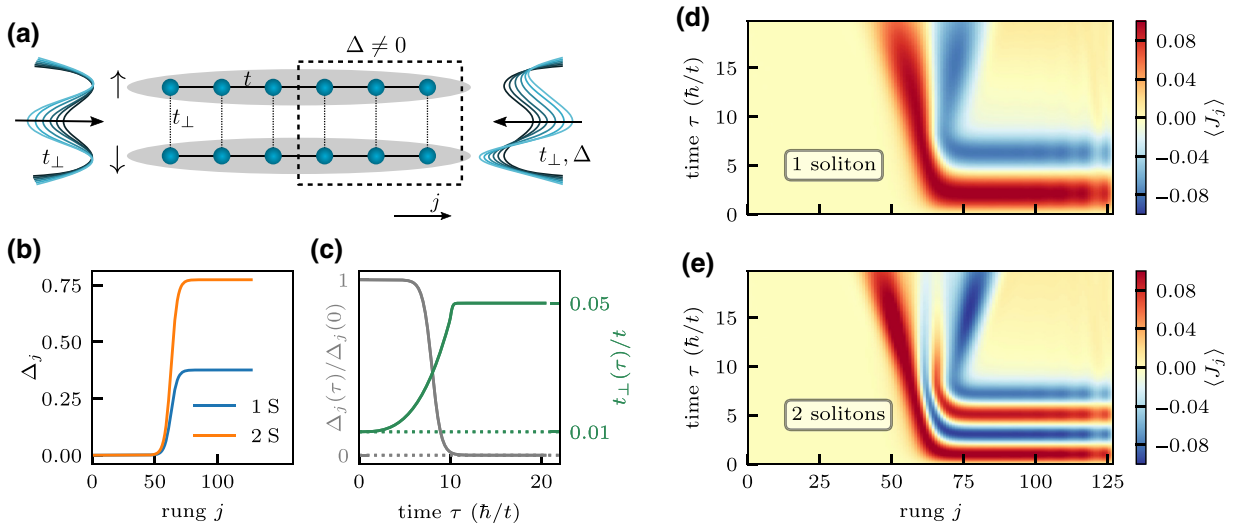

FIG. 1. The creation of solitons in coupled Bose-Hubbard chains. (a) A soliton can be created by applying a chemical-potential gradient between the two chains in one half of the system $\sum_j \Delta_j(\tau)(n_{j\uparrow} - n_{j\downarrow})$, as indicated by the dashed region. Ramping up the tunnel coupling $t_\perp$ simultaneously, which decreases the barrier on the rung, enables us to further stabilize the phase-imprinting process. (b) The spatial profile of the applied chemical-potential gradient Δ_j for the preparation of one (1S) and two (2S) solitons. (c) The time dependence of the chemical-potential difference Δ_j and tunnel coupling $t_\perp$. (d),(e) The resulting profiles of the mean local current $\langle J_j \rangle$ suggest the creation of one (d) and two (e) solitons, respectively. The time evolution is performed with the TEBD algorithm for bond dimension $\chi = 1000$ and $L = 128$ rungs.

in a previous theoretical work [24], we have shown that the sine-Gordon model describes the low-energy physics of two coupled spin chains very well, identifying an experimental realization of such a setup and developing the measurement protocols to extract the information of the emergent field theory remain unaddressed challenges that motivate our present work.

Here, we show how solitons, which are the fundamental excitations of the sine-Gordon model, can be created in a setting of ultracold bosons trapped in an optical lattice [see Fig. 1(a)]. The solitons are most directly observed when measuring the current between the chains by first applying beam-splitter operations and then taking snapshots with a quantum gas microscope. Using similar beam-splitter operations, we furthermore show how the full counting statistics of the topological charge, which counts the number of excited solitons, can be obtained. We use numerical simulations based on matrix product states, to assess the experimental requirements of the proposed protocols.

The paper is organized as follows. In Sec. II, we briefly introduce the sine-Gordon model and its realization using coupled 1D Bose-Hubbard chains. The creation of a soliton is discussed in Sec. III. In Sec. IV, we present a detection method to capture the topological charge of solitons. The requirements for the experimental preparation of a low-energy state of the sine-Gordon field theory are discussed in Sec. V. Our conclusions are presented in Sec. VI and the appendixes contain a couple of technical details.

II. TUNNEL-COUPLED BOSE-HUBBARD CHAINS

The sine-Gordon model emerges as the low-energy description of two tunnel-coupled interacting 1D systems. Here, we consider two identical Bose-Hubbard chains with Hamiltonians $H_\uparrow^{\mathrm{BH}}$ and $H_\downarrow^{\mathrm{BH}}$, coupled with a tunneling term $H_\perp$. The dynamics are therefore set by the total Hamiltonian $H = H_\uparrow^{\mathrm{BH}} + H_\downarrow^{\mathrm{BH}} + H_\perp$. Here,

$$H_\alpha^{\mathrm{BH}} = -t\sum_{j=0}^{L-2}(b_{j\alpha}^\dagger b_{j+1\alpha} + \mathrm{h.c.}) + \frac{U}{2}\sum_{j=0}^{L-1} n_{j\alpha}(n_{j\alpha} - 1), \tag{1}$$

where $b_{j\alpha}$ ($b_{j\alpha}^\dagger$) annihilates (creates) a boson on rung j in chain $\alpha = \{\uparrow, \downarrow\}$ and $n_{j\alpha} = b_{j\alpha}^\dagger b_{j\alpha}$ is the density. The tunnel coupling Hamiltonian reads

$$H_\perp = -t_\perp \sum_{j=0}^{L-1}(b_{j\uparrow}^\dagger b_{j\downarrow} + \mathrm{h.c.}). \tag{2}$$

We use open boundary conditions throughout our work. The derivation of the low-energy description of the coupled wires closely follows the original proposal [25]. We consider each of the chains to be at noninteger filling to realize a superfluid state for arbitrary values of the hopping t and the interaction strength U.

In the absence of interchain coupling $t_\perp = 0$, the low-energy behavior is obtained by bosonization. One first introduces the phase field $\phi_\alpha(x)$ and its conjugate field $\Pi_\alpha(x)$. These two fields are related to the microscopic operators as $b^\dagger_{j,\alpha} \simeq \gamma e^{i\phi_\alpha(x)}$ and as $n_{j,\alpha} \simeq n + \Pi_\alpha(x)$, respectively, where γ is a nonuniversal prefactor and n is the average density. Within bosonization, the two 1D chains are governed by the Luttinger-liquid Hamiltonian

$$H^{\mathrm{LL}}_\alpha = \int dx \frac{\hbar v_s}{2}\left(\frac{\pi}{K}\Pi^2_\alpha(x) + \frac{K}{\pi}(\partial_x\phi_\alpha(x))^2\right), \qquad (3)$$

where, K is the Luttinger parameter and v_s is the sound velocity. The Luttinger parameter is larger than one, $K \geq 1$, for repulsive interactions $U > 0$ [9] and approaches $K = 1$ in the limit of infinite repulsive interactions $U/t \to \infty$. For weak tunneling $t_\perp \ll t$, the interchain coupling can be reintroduced perturbatively [25]. Upon bosonizing, the transverse Hamiltonian reads as $H_\perp = -2|\gamma|^2 t_\perp \int dx \cos(\phi_\uparrow - \phi_\downarrow)$. Performing a rotation to symmetric $\psi = \phi_\uparrow + \phi_\downarrow$ and antisymmetric $\phi = \phi_\uparrow - \phi_\downarrow$ degrees of freedom results in the explicit decoupling of the two sectors. The symmetric combination is governed by a gapless Luttinger liquid and the sine-Gordon field theory given in Eq. (4) emerges for the relative degree of freedom ϕ:

$$H^{\mathrm{SG}} = \int dx\, \frac{\hbar v_s}{2}\left(\frac{2\pi}{K}\Pi^2 + \frac{K}{2\pi}(\partial_x\phi)^2\right) - 2t_\perp|\gamma|^2\cos\phi. \qquad (4)$$

The integrability of the sine-Gordon model allows for an exact determination of its particle content, together with an analytical expression for the two-body scattering matrix [13]. The fundamental excitations are topological solitons and antisolitons, for which the phase field ϕ interpolates between the degenerate minima of the $\cos\phi$ interaction. Therefore, the phase field ϕ winds up by 2π when traversing a soliton. These quasiparticles have a relativistic dispersion law $E_s(k) = \sqrt{v_s^4 M^2 + v_s^2 k^2}$. The soliton mass M has a complicated dependence on the bare parameters of the Hamiltonian [37] but scales with the transverse hopping $t_\perp$ in a rather simple manner $M \propto t_\perp^{\frac{2K}{4K-1}}$.

Depending on the interaction K, solitons and antisolitons can form bound states of infinite lifetime, which are called breathers. The interaction K sets the number of breathers in the excitation spectrum, $N = \lfloor 4K - 1 \rfloor$, and their mass as $M_{B_n} = 2M\sin\left(\frac{\pi}{2}\frac{n}{4K-1}\right)$. Crucially, when K is increased, the relative mass difference between two consecutive breathers is reduced: in the limit of large K, or weak interactions, the mass spectrum of the breather collapses to a continuum and the quantum model is well approximated by the classical sine-Gordon theory [35,38,39]. In contrast, the deep quantum regime of the field theory is realized when only few breathers are present in the spectrum. In tunnel-coupled Bose-Hubbard chains, strong interactions can be achieved by quenching the kinetic energy of the atoms. Thereby, Luttinger parameters K of order one are reachable when considering noninteger fillings, which avoids the Mott-insulating regimes. To this end, we focus in our numerical simulations presented below on the regime of infinitely strong interactions, corresponding to $K = 1$. Deviations from this regime lead to changes in the microscopic parameters of the field theory. However, the qualitative behavior remains. In the infinitely repulsive regime, the Bose-Hubbard ladder maps to coupled Heisenberg chains. In such spin chains, the regime of validity of the sine-Gordon description has been thoroughly analyzed in Ref. [24].

III. CONTROLLED SOLITON IMPRINTING

Creating, manipulating, and detecting the fundamental excitations of an emergent sine-Gordon field theory is a challenge. One possibility is to act on the microscopic model with an inhomogeneous perturbation such that the ground state of the emergent field theory hosts initially localized solitons. Proposals for achieving this are based on Raman-coupled quasicondensates [40] and have motivated further theoretical analysis of the propagation of solitons [41,42]. By contrast, for the experimental realization that we are proposing, the goal is to prepare the ground state of the field theory and subsequently to dynamically imprint the soliton.

In this section, we propose the protocol for imprinting a soliton on the exact ground state of the two tunnel-coupled Bose-Hubbard chains. Protocols for approximately realizing the ground state are discussed in Sec. V. Our strategy aims at carefully tuning the spatial profile of the relative phase $\phi(x)$ such that it undergoes a 2π phase slip when traversing the system. In order to avoid a massive creation of excitations during the preparation, smooth and slow parameter changes are paramount.

We begin by introducing a space-time-dependent chemical-potential gradient between the two chains $H \to H + \sum_j \Delta_j(\tau)(n_{j\uparrow} - n_{j\downarrow})$ that induces a relative phase drift between the two halves of the system [29]. This is best seen from bosonizing the density gradient $(n_{j\uparrow} - n_{j\downarrow}) \to \Pi(x)$. The sine-Gordon Hamiltonian thus gets an additional term $H^{\mathrm{SG}} \to H^{\mathrm{SG}} + \int dx\, \Delta(\tau,x)\Pi(x)$, leading to a deformed equation of motion $\partial_t\phi = \frac{v_s\pi}{K}\Pi + \Delta(\tau,x)$, where $\Delta(\tau,x)$ denotes the potential imbalance in the continuum limit. The gradient $\Delta(\tau,x)$ hence acts as a source for the accumulation of the relative phase ϕ. When winding up the phase in half of the system, while leaving the other untouched, a relative phase difference of 2π can be achieved. This configuration is then stabilized by the cosine potential of the relative phase in the sine-Gordon model given in Eq. (4). At this point, the potential imbalance needs to be switched off in the preparation protocol.

To prevent the phase from slipping into the next minimum or from oscillating strongly, we simultaneously deepen the potential barrier by increasing the interchain hopping $t_\perp$, which helps to pin down the phase to the desired value. The result of our protocol is the creation of a localized wave packet of excitations, primarily containing the desired number of solitons. The wave packet is approximately contained within the regions where the chemical-potential gradient $\partial_x \Delta(\tau, x)$ is not zero. A graphical summary of the soliton-creation protocol can be found in Figs. 1(b) and 1(c).

Within bosonization, the rung current is proportional to the sine of the relative phase: $J_j \equiv -ib^\dagger_{j\uparrow} b_{j\downarrow} + ib^\dagger_{j\downarrow} b_{j\uparrow} \simeq 2|\gamma|^2 \sin\phi$. We can thus optimize the parameters of the protocol by measuring the current between the two rungs and requiring a smooth sine-shaped profile without additional oscillations [see Figs. 1(d) and 1(e)]. The data are obtained numerically using the time-evolving block-decimation (TEBD) algorithm [43] for two coupled Bose-Hubbard chains of length $L = 128$ at filling $n = 1/8$ and Luttinger parameter $K = 1$. In Appendix A, we show the current profiles for different filling fractions. Depending on the strength of the chemical-potential gradient, we can also control the number of zero crossings in the current profile. Therefore, our data suggest that a quantized number of solitons can be created in the quantum limit of the sine-Gordon theory in a controlled way using this protocol.

Furthermore, we numerically compute the energy of the state before and after the soliton imprinting. For the data shown in Figs. 1(d) and 1(e), we find that the additional energy is $\Delta_{1S} = 0.50t$ and $\Delta_{2S} = 0.92t$. This should be compared to the cost of creating a soliton measured by the energy gap. For $K = 1$, one has that the dispersion relations of the soliton and the first breather are equal: $E_{B_1} = E_S$. Hence, we can extract the energy of the soliton by measuring the energy of the lowest breather in the spectral function [24]. From that, we estimate $E_S(k = 0) = (0.24 \pm 0.04)t$. Therefore, slightly more energy is pumped into the system by the preparation protocol, which is reasonable, as there will also be excitations of the gapless symmetric modes and, furthermore, slightly dispersing wave packets of the solitons are created. Nonetheless, it would be desirable to have access to other more direct observables to characterize the solitons.

One approach could be to track the phase from individual snapshots of the current and locate phase jumps therein. This strategy has been successfully applied deep in the semiclassical limit, characterized by a large Luttinger parameter K for coupled quasicondensates [27], where solitons have a large spatial extent and can therefore be directly imaged. In the setting considered here, however, the local current can only take three values, $+, 0, -$, depending on the configuration of the hardcore bosons on a single rung. Even in the case of finite Hubbard interactions, the local current is still quantized to integer values.

Therefore, coarse graining over spatially extended regions has to be performed. It is crucial that averaging on scales larger than the soliton itself has to be avoided, because then the phase slip cannot be resolved either. We estimate the size of the soliton using a classical soliton profile that at rest obeys $\ell \partial_x \phi = \sqrt{1 - \cos\phi}$, with $\ell = 2\hbar K/(\pi v_s M)$. For $K = 1$ and $n = 1/8$, we obtain $M v_s^2 \simeq 0.25t$, giving $\ell \simeq 2$ lattice sites. From these estimates, it can be deduced that the phase profile of the soliton cannot be directly extracted, as coarse graining is required to resolve the phase, but the soliton itself is very localized in space. This is a direct consequence of being deep in the quantum regime of the sine-Gordon model.

To confirm this picture, we perform numerically projective measurements of the current: upon coarse graining, all phase slips are averaged out rapidly (see Appendix B). Due to the small size of the classical soliton, one may question the validity of the field-theory description. However, it should be emphasized that the classical estimate is only a rough qualitative indicator. Indeed, a careful quantitative study of coupled spin chains [24] shows that the sine-Gordon model is indeed a faithful description of strongly interacting ladder systems. As an alternative to characterize and count the solitons, we propose instead to investigate the topological charge.

IV. DETECTING SOLITONS FROM THE TOPOLOGICAL CHARGE

Among the infinite set of conservation laws of the sine-Gordon model, 'which arise from integrability [12,44], is the topological charge, which is an integral over a total derivative,

$$Q = \int \frac{dx}{2\pi}\, \partial_x \phi(x). \tag{5}$$

Using the canonical commutation relations $[\phi(x), \Pi(y)] = i\delta(x - y)$, one can readily obtain $[Q, H^{\mathrm{SG}}] = 0$. The topological charge is quantized in integer units: each soliton contributes $+1$, antisoliton -1, and breathers, which are bound states of a soliton and an antisoliton, do not contribute at all. For our analysis, it is useful to introduce the accumulated topological charge $Q(x) = \int^x \frac{dy}{2\pi} \partial_y \phi$, which is only conserved (and quantized) as $x \to \infty$. The accumulated topological charge has the advantage that it is automatically coarse grained over a large portion of the system.

Our goal is now to find a microscopic realization of the accumulated topological charge. To this end, it is useful to introduce the local current $J_j = (-ib^\dagger_{j\uparrow} b_{j\downarrow} + \mathrm{h.c.})$ and energy $E_j = (b^\dagger_{j\uparrow} b_{j\downarrow} + \mathrm{h.c.})$ operators acting on a single rung. Using bosonization, the topological charge density can be identified as the most relevant contribution to the

following combined observable:

$$E_j J_{j+1} - J_{j-1} E_{j+2} \simeq 8|\tilde{\gamma}|^4 \partial_x \phi. \tag{6}$$

The energy operators are measured on even rungs and currents on odd ones and $\tilde{\gamma} \simeq \gamma$; a possible difference between the two may arise due to UV field-theory renormalization. The actual value of $\tilde{\gamma}$ is, however, unimportant for us. With this identification, we can readily introduce a lattice version of the accumulated topological charge as

$$\begin{aligned} Q_j &\equiv \sum_{i \text{ even}}^{j} (E_i J_{i+1} - J_{i-1} E_{i+2}) \simeq 16\pi |\tilde{\gamma}|^4 Q(x) \\ &= 16\pi |\tilde{\gamma}|^4 [\phi(x) - \phi(0)]. \end{aligned} \tag{7}$$

We numerically evaluate this lattice regularization of the topological charge for the state with one and two solitons, respectively, discussed in Sec. III (see Fig. 2). The accumulated topological charge captures the phase difference between a given site in our system and the left boundary. The chemical-potential gradient Δ_j is chosen to act on the right half of the system. Therefore, the left boundary does not evolve and $\phi(0)$ is a mere constant. As a consequence, Q_j probes the dynamics of the field $\phi(x)$. We find that during the soliton-creation process ($\tau < 10\hbar/t$), the value of the topological charge is still drifting. However, as the soliton-creation process has finished, the topological charge remains remarkably stable in time, as demonstrated by the plateau in Fig. 2. By comparing the one-soliton and two-soliton imprinting, shown in Figs. 2(a) and 2(b), respectively, we observe that the total phase slip of the two-soliton state is about twice that of the one-soliton state, as expected. The stability of the soliton is a clear signature of the emergent sine-Gordon field theory, because the accumulated charge is just a sum of local energy and current operators, without any evident topological property. Thus the presence of the underlying soliton is quite remarkable.

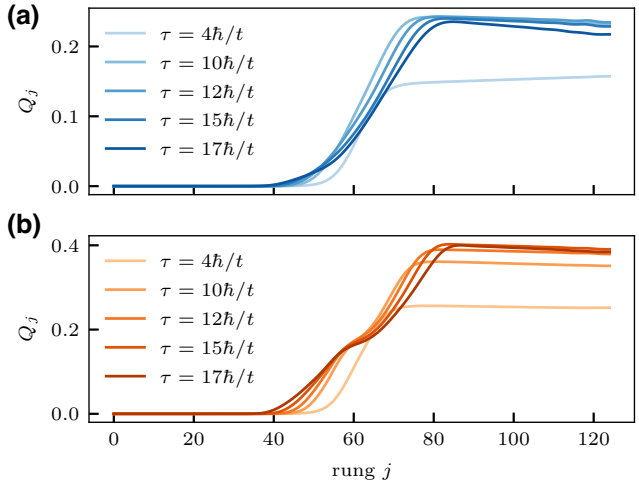

FIG. 2. The accumulated topological charge, shown for (a) one soliton and (b) two solitons at various times (legend). The soliton-creation protocol and system size are the same as in Fig. 1 and take a total time of $10\hbar/t$. Thus, for the earliest times shown, the imprinting has not yet completed. Once the solitons have been created, the total topological charge remains remarkably constant. The lattice regularization of the topological charge is not quantized to unity, due to the nonuniversal prefactor $\tilde{\gamma}$ in Eq. (7). However, the topological charge for the two solitons in (b) is approximately twice that of the single soliton in (a), indicating a quantization of the excitation.

The topological charge density as defined in Eq. (6) can be directly measured with quantum gas microscopes [45]. To this end, a proper local basis rotation has to be performed with beam-splitting operations on individual rungs of the Bose-Hubbard ladder. The simpler operator is the current, which can be obtained as follows [46]. After the hopping between the rungs is frozen by strongly increasing the depth of the optical lattice, each of the individual rungs are evolved in time for a duration of $\pi/4$. This realizes a unitary $U_j^J = \exp(i\frac{\pi}{4} E_j)$ which transforms the relative density to the rung current

$$(U_j^J)^\dagger (n_{j\downarrow} - n_{j\uparrow}) U_j^J = J_j. \tag{8}$$

Here, crucially, we assume the absence of double occupancies. In the case of infinite repulsion, which we consider, this is trivially the case. However, real double occupancies can also be neglected in the experimentally accessible limit of strong but finite interactions, because we are focusing on the dilute limit and strong interactions. As an alternative, arbitrary occupancies of the double well are allowed if one switches off the interactions during the rotation by, e.g., Feshbach resonances.

In a similar way, the rung energy E_j can be transformed to the relative density by first applying a potential imbalance, which couples to the density difference, for period $\pi/4$ and then applying the beam-splitter operation, leading to $U_j^E = U_j^J \exp[i\frac{\pi}{4}(n_{j\uparrow} - n_{j\downarrow})]$. This transformation maps the density difference to the local energy density

$$(U_j^E)^\dagger (n_{j\uparrow} - n_{j\downarrow}) U_j^E = E_j. \tag{9}$$

By first applying a potential gradient on every even rung and then applying the beam-splitter operation U^J globally, as depicted in Fig. 3(a), projective measurements in the density basis yield the staggered string operators '$J_0 E_1 J_2 E_3 J_4 E_5 \cdots$'. From those, the accumulated charge Q_j given in Eq. (7) is then obtained directly. By numerically sampling snapshots after performing the beam-splitter operations [47,48], we generate the full counting statistics of the topological charge (for details, see Appendix C). The average over the accumulated topological charge over 8000 snapshots is shown in Fig. 3(b),

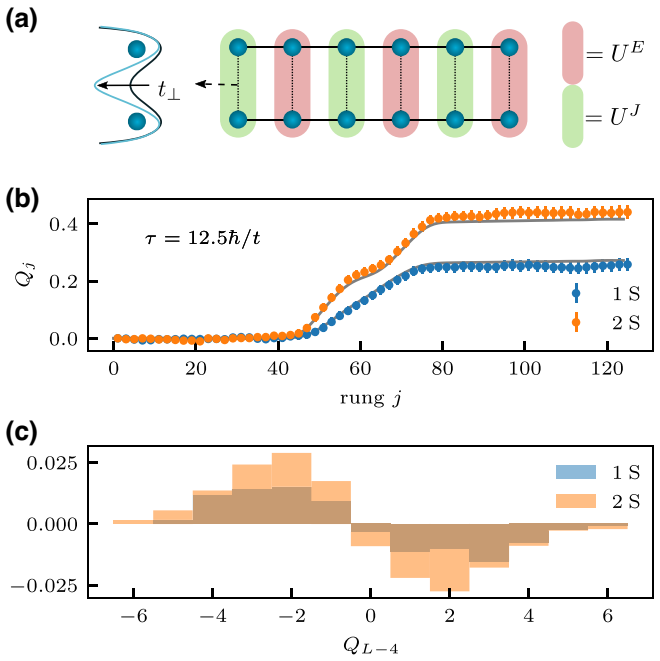

FIG. 3. Snapshots of the topological charge. (a) After freezing the hopping within the chain, a density gradient is applied for a period of $\pi/4$ to even sites (pink), followed by a global beam-splitter tunneling operation for a time $\pi/4$. This is effectively described by the unitaries U^J and U^E. (b) The accumulated topological charge extracted from the snapshots for the one- and two-soliton states prepared as in Fig. 1. The average is taken over approximately 8000 snapshots. The error bars represent the standard error of the mean and the gray line is the expectation value of the state. (c) The differential histograms of the total topological charge between the soliton states and the ground state. Deep in the quantum regime, the soliton manifests itself in the skewness of this distribution.

where we find good agreement with the direct measurement of the state. Moreover, we show a difference of the full distribution function of the topological charge Q_{L-4} for a state in which solitons are prepared compared to the ground state, which does not carry any solitonic excitations [see Fig. 3(c)]. We note that the x axis of this histogram is quantized to integer values, as Q_j is an integer when it is taken from a single snapshot. Deep in the quantum regime, the soliton manifests itself as a skewness in the broad distribution of Q_j. Deep in the classical regime, by contrast, the full distribution function of the topological charge would exhibit a sharp peak.

V. GROUND-STATE PREPARATION

So far, we have assumed that the ground state of the coupled chain has already been prepared. Here, we suggest an adiabatic ground-state preparation protocol that can be implemented using ultracold atoms in optical lattices with tunable local potentials. The finite-mass gap of the sine-Gordon field theory and the decoupling between the symmetric and antisymmetric sector at low energies enable us to prepare the sine-Gordon ground state in reasonable time. Of course, this only remains true as long as the sine-Gordon model is a good description of the coupled chains, which may not be always the case during the state-preparation process.

We propose the following adiabatic ground-state protocol for creating an approximate ground state of the two tunnel-coupled Bose-Hubbard chains at filling $n = 1/2$:

(i) Initialize a single chain with unit filling while the intrachain hopping is switched off.
(ii) Split the potential on every site to prepare the ground state of a single particle in a double well.
(iii) Linearly ramp up the intrachain hopping t to spread correlations through the system.

We simulate this ground-state preparation protocol numerically using matrix product states [see Fig. 4(a)]. To this end, we start out from the ground state of each rung and then increase the intrachain hopping t over a duration of $50\hbar/t$, such that the ratio of the inter- and intrachain hopping is $t_\perp/t = 0.2$ at the end of the protocol. We do not attempt to optimize these numbers too carefully. Rather, this should be seen as a guide for the approximate requirements of the adiabatic state-preparation protocol.

The whole system is gapless due to the symmetric degrees of freedom. Hence a large amount of energy is injected into the system even for slow protocols. However, the symmetric modes are expected to quickly decouple from the sine-Gordon Hamiltonian, which in turn has a finite-mass gap. Therefore, the antisymmetric sector remains close to its ground state overall. The total energy is thus not a good indicator of the quality of the sine-Gordon state preparation, due to the large contribution from the symmetric modes.

In order to assess the quality of the adiabatically prepared state, it can, for example, be probed spectroscopically (see Appendix D). We find numerically that the low-energy excitations as measured by the spectral function are in good agreement with the spectral function evaluated from the exact ground state. This demonstrates that the asymmetric sector is well prepared using this procedure.

In addition, we can even imprint a soliton on top of the adiabatically prepared ground state, following our suggestion discussed earlier in Sec. III [for details, see Figs. 4(b) and 4(c)]. The resulting current profiles are again indicative of having a soliton imprinted [see Fig. 4(d)]. Furthermore, this is supported by a reasonably stable accumulated topological charge [see Fig. 4(e)]. This demonstrates that the adiabatically prepared ground state has the essential features of the ground state of the emergent sine-Gordon field theory.

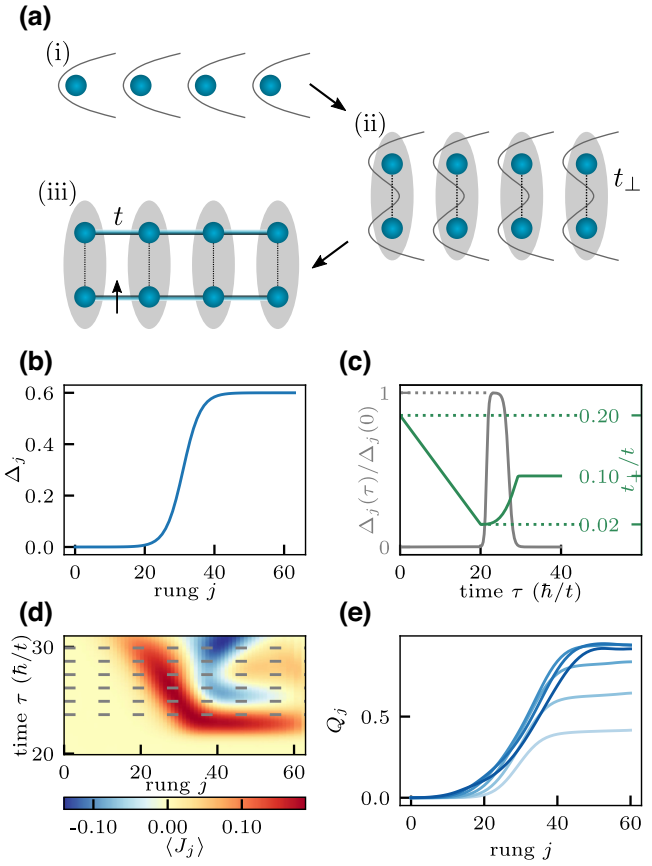

FIG. 4. The adiabatic ground-state preparation. (a) The ground-state preparation protocol starts out as a 1D Mott insulator with negligible hopping, $t \approx 0$. Then, the tube is split adiabatically into two, realizing the ground state on each of the single rungs. Now, correlations build up across the system by adiabatically ramping up the intrachain hopping t over a time $50\hbar/t$, such that after completing the process, $t_\perp/t = 0.2$. (b),(c) The subsequent soliton-imprinting protocol is closely related to the one discussed previously. Before applying the chemical-potential-gradient profile (b), however, we first lower $t_\perp/t$ from 0.2 to 0.02 (c). The gray steplike function then shows the time interval during which the relative phase is accumulated. (d) Current profiles around the soliton-imprinting stage. (e) The accumulated topological charge shown at time slices indicated by the gray dashed lines in (d). The lightest shade represents the earliest time and the darkest one the latest.

VI. CONCLUSION AND OUTLOOK

The sine-Gordon field theory emerges as the effective description in a wealth of physical systems. Here, we propose access to the deep quantum regime of the sine-Gordon model by realizing tunnel coupled Bose-Hubbard chains. We discuss adiabatic ground-state preparation protocols, as well as protocols for creating the fundamental excitations—the solitons—of the sine-Gordon model. The soliton can be most directly seen in the interchain current and the topological charge, both of which can be measured with quantum gas microscopes using beam-splitter operations.

For future work, it would be interesting to explore scattering of solitonic wave packets. Fundamental information about the excitations and their mutual interactions can be extracted from scattering events. Information about the integrable field theory can thereby be obtained, in which the multiparticle scattering processes are rather peculiar [12,13,24]. Moreover, it would be exciting to find ways to create initial states with a finite density of solitons. In such a true many-body regime, the thermalization dynamics [14] and the emergent generalized hydrodynamics [16,49,50] of the strongly interacting sine-Gordon field theory could be explored.

The raw data and the data analysis are available on Zenodo [52].

ACKNOWLEDGMENTS

We thank F. Essler for useful discussions. The matrix-product-state simulations were performed using the TeNPy package [51]. We acknowledge support from the Deutsche Forschungsgemeinschaft (DFG, German Research Foundation) under Germany's Excellence Strategy EXC 2111–390814868 and DFG Grants No. KN1254/1-2, KN1254/2-1, the European Research Council (ERC) under the European Union Horizon 2020 research and innovation program (Grant Agreement No. 851161), as well as the Munich Quantum Valley, which is supported by the Bavarian state government with funds from the Hightech Agenda Bayern Plus.

APPENDIX A: SOLITON PROFILES AT DIFFERENT DENSITIES

We compare the soliton profiles and the accumulated topological charge obtained for states at different densities (see Fig. 5). Apart from tuning the strength of the chemical potential, we also reduce the imprinting time with increasing density. Concretely, the time scales for imprinting are chosen to be inversely proportional to the density to compensate for the higher sound velocity in systems with higher density. We also numerically find that for a higher density, the soliton is more dispersive (see Fig. 5).

We also evaluate the accumulated topological charge, which depends approximately linearly on the density [see Figs. 5(d)–5(f)]. There are small drifts of the topological charge in time, signaling a weak breaking of the conservation law of the total topological charge. As previously pointed out, the conservation of the topological charge is not directly implemented in the coupled Hubbard chain but emerges from the effective field theory. Furthermore, this confirms that the parameter regime of Fig. 2 realizes a high-quality sine-Gordon soliton, while more important corrections beyond sine-Gordon are present at higher densities, as shown in Fig. 5. One reason for the worse stability

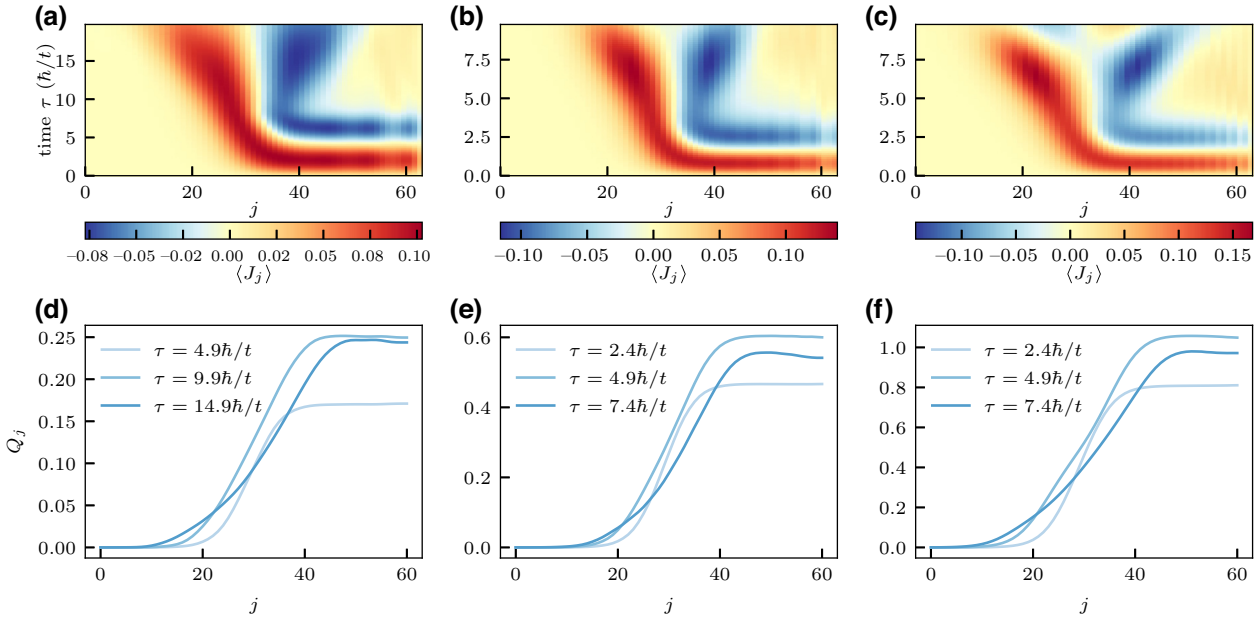

FIG. 5. Solitons at different densities. (a)–(c) The current profiles when applying the soliton-creation protocol for different densities in the initial ground state of $L = 64$ rungs: (a) $n = 1/8$, (b) $n = 1/4$, and (c) $n = 1/2$. The soliton spreading is significantly faster for higher densities due to the larger sound velocity. (d)–(f) The corresponding accumulated topological charge for some time slices: (d) $n = 1/8$, (e) $n = 1/4$, and (f) $n = 1/2$.

is the reduced preparation time, which is required due to the increased sound velocity, while keeping the system size fixed. It would be interesting to optimize the soliton imprinting to further reduce these undesired effects in future work.

APPENDIX B: ATTEMPTING TO EXTRACT THE PHASE OF THE SOLITON FROM CURRENT SNAPSHOTS

In this appendix, we directly analyze the snapshots of the current $J_j = (-ib^\dagger_{j\uparrow} b_{j\downarrow} + \text{h.c.})$ and show that deep in the quantum regime, one cannot extract the phase directly upon coarse graining. As we discuss in the main text, the reason is that in this regime the soliton itself is of very small extent and hence is averaged out upon coarse graining. Let us describe the formal procedure here. Within bosonization, the current operator can be written in terms of the phase field as

$$J \simeq 2|\gamma|^2 \sin(\phi), \tag{B1}$$

where γ is a nonuniversal prefactor. When taking snapshots of the current $JJJJ\ldots$, it is conceivable in principle that one can extract the phase profile in space. The challenges are the following: first, a reliable estimate of the nonuniversal prefactor γ is needed; and, second (and more importantly), coarse graining has to be performed to obtain the phase. A snapshot of the current on the ladder takes the values

$$N_{j\downarrow} - N_{j\uparrow} \in \{-1, 0, 1\}, \tag{B2}$$

where $N_{j\alpha} = 0, 1$ is the measurement outcome of $n_{j\alpha}$. We do not consider higher occupancy as we are in the limit $K \to 1$ and at low average filling. We then coarse grain the current over a certain number of sites and invert the relation shown in Eq. (B1) while flattening the grouped current with the value of $2|\gamma|^2$. We extract a value of $2|\gamma|^2 \approx 0.7$ from the spectral function; however, the exact value does not considerably affect the outcome of the procedure. There is always an ambiguity in the inversion of Eq. (B1): we choose to make a "jump" in the phase when the absolute value of the current hits its maximum (here, taken to be 0.7) once. Another maximum with the same sign corresponds to a jump back. In Figs. 6(a) and 6(c), we show 20 snapshots of the coarse-grained current,

$$\overline{J_j} = \frac{1}{N} \sum_{i=0}^{N-1} (N_{i+j\downarrow} - N_{i+j\uparrow}) \tag{B3}$$

over $N = 4$ and $N = 6$ sites, respectively. In Figs. 6(b) and 6(d), we then show the extracted phase

$$\overline{\phi_j} = \arcsin\left(\frac{\overline{J_j}}{2|\gamma|^2}\right), \tag{B4}$$

where $\overline{J_j}$ is thus flattened to $2|\gamma|^2$ in the event that $\overline{J_j} > 2|\gamma|^2$. From this, it is already clear that the rare phase

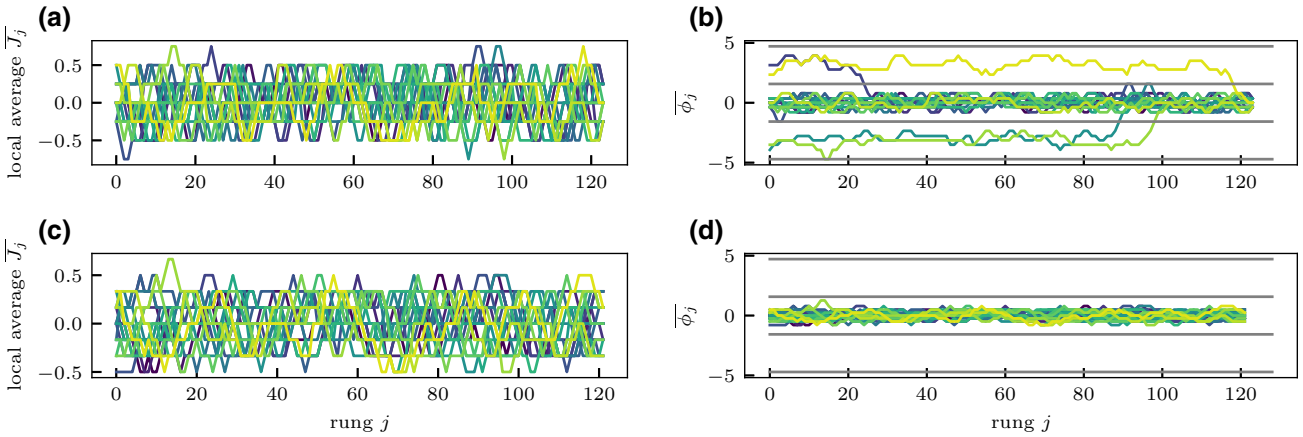

FIG. 6. Snapshots of the coarse-grained current. (a),(c) Illustrations of 20 snapshots of the coarse-grained current for (a) $N = 4$ and (c) $N = 6$ grouped sites of the one-soliton state, respectively. There are huge fluctuations in these data because we are considering the deep quantum regime of the emergent sine-Gordon theory. (b),(d) The relative phase extracted from the snapshots of the current. The rare jumps that are present for (b) $N = 4$ disappear when taking (d) $N = 6$. The horizontal gray lines are drawn at $\pm\pi/2$ and $\pm 3\pi/2$. The snapshots are obtained from the one-soliton state, presented in Fig. 1, at time $\tau = 12.5\hbar/t$.

jumps disappear completely upon coarse graining over a couple of sites. In the random subset of 20 snapshots that are shown, there is not even a single one that winds up a phase of 2π according to our procedure when grouping $N = 6$ sites.

In order to have a larger sample size of snapshots, we create a histogram of the phase accumulation obtained in around 40 000 snapshots [see Figs. 7(a) and 7(b)]. These histograms are symmetric and do not show special features. To strengthen this point, we plot the differential histograms between the ground state and the state containing one soliton [see Figs. 7(c) and 7(d). Except for statistical fluctuations, we find that there is no difference between these states. This illustrates that no special features can be obtained from the coarse-grained data. Taking the estimated size of the soliton of two lattice sites, which we give in the main text, this finding is not surprising. It just reflects the fact that the regime we are considering is dominated by quantum fluctuations.

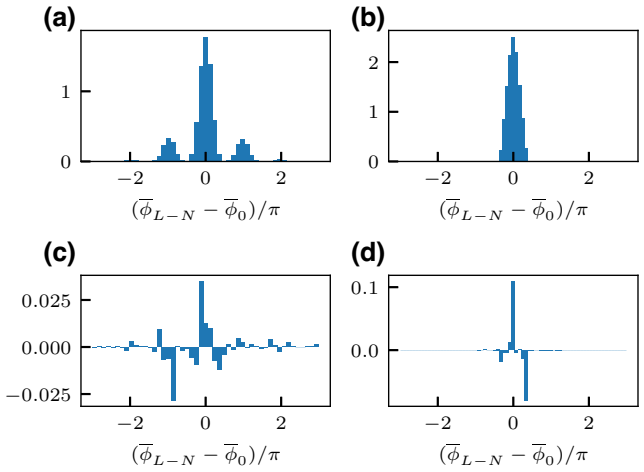

FIG. 7. (a),(b) Histograms of the phase accumulation across the system obtained from approximately 40 000 snapshots of the one-soliton state for (a) $N = 4$ and (b) $N = 6$ grouped sites, respectively. (c),(d) The differential histograms comparing the soliton data to the ground state: (c) $N = 4$ and (d) $N = 6$.

APPENDIX C: EXTRACTING THE TOPOLOGICAL CHARGE FROM SNAPSHOTS

In this appendix, we show more in detail how to extract the soliton profile from snapshots of the topological charge density. After performing the rotations corresponding to U^J and U^E [see Eqs. (8) and (9), respectively] and taking the snapshots in that basis, $JEJE\ldots$, we can reconstruct the expectation values of $\langle J_j E_{j+3}\rangle$ (for even j) and $\langle E_j J_{j+1}\rangle$ (for odd j). These are shown in Fig. 8(a). These expectation values deviate from zero around the position of the soliton. Then, taking the difference corresponds to the topological charge density, which exhibits a bump at the position of the soliton [see Fig. 8(b)]. Taking the cumulative sum then reveals the accumulated topological charge, which is quantized when traversing the full system [see Fig. 8(c)].

APPENDIX D: BREATHER SPECTROSCOPY OF THE ADIABATICALLY PREPARED STATE

Here, we analyze the breather spectrum of the adiabatically prepared ground state following the protocol of Sec. V and compare it to the spectrum of the exact ground state on the coupled chains. To this end, we compute the

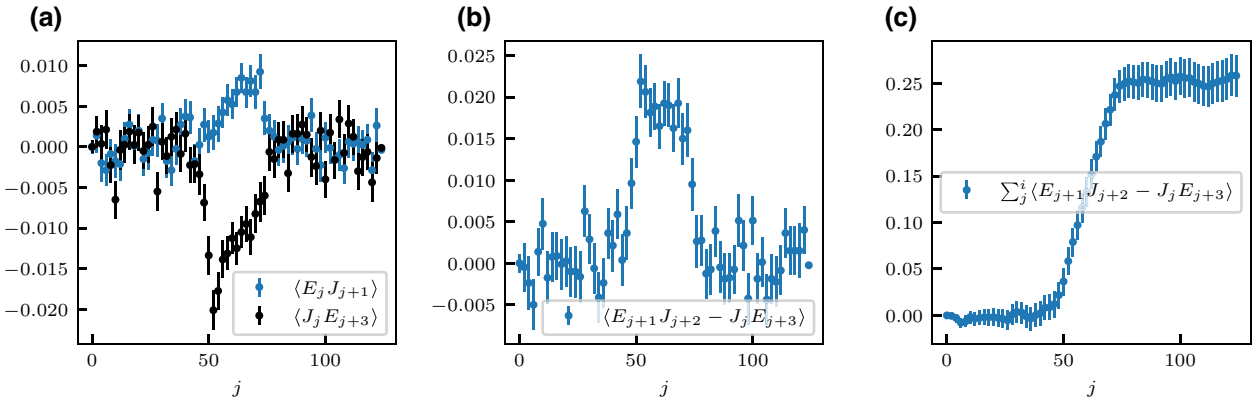

FIG. 8. Snapshots for determining the topological charge. (a) The average data extracted from the snapshots. For an odd rung index j, we show $E_i J_{i+1}$, and for an even rung index j, we show $J_j E_{i+3}$. These expectation values deviate from zero around the position of the soliton. The averages are taken over $N \approx 8000$ snapshots. (b) From the difference between the two expectation values, we compute the topological charge density. (c) The cumulative profile of topological charge density then gives the topological charge Q_j.

spectral function at momentum $k = 0$,

$$S(\omega, k = 0) \sim \int dt e^{i\omega t} \sum_{n=0}^{L-1} \langle O_n(t) O_{L/2} \rangle \tilde{\psi}_0, \qquad \text{(D1)}$$

where $|\tilde{\psi}_0\rangle$ is the (adiabatically prepared) ground state. The operators O_n are defined on the rungs, to couple to the asymmetric sector in which the sine-Gordon theory is emerging. We observe a nice correspondence between the spectral functions and the expected breather energies (see Fig. 9). Data are shown for three different operators: (i) $O_i = b^\dagger_{i\uparrow} b_{i\downarrow}$, coupling to all breathers; (ii) $O_i = b^\dagger_{i\uparrow} b_{i\downarrow} + \text{h.c.}$, coupling to the even breathers only; and (iii) $O_i = i b^\dagger_{i\uparrow} b_{i\downarrow} + \text{h.c.}$, coupling to the odd breathers.

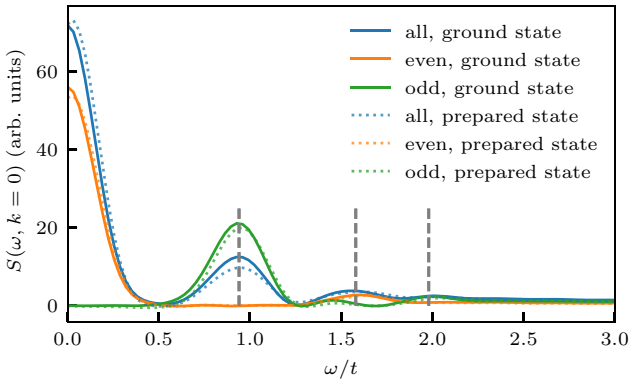

FIG. 9. The breather spectroscopy. The spectral function at zero momentum, $k = 0$, as defined in Eq. (D1), is computed for the ground state and the adiabatically prepared ground state at $t_\perp/t = 0.2$. This state is prepared as described in the main text for a system of $L = 32$ rungs within a time of $50\hbar/t$. The spectrum is computed separately for the different parity sectors of the breather. The gray dashed lines show the location of the exact energies of the three breathers present for $K = 1$. The spectra are in very good agreement, demonstrating that the ground state of the antisymmetric sector is well prepared by our procedure.

[1] S. Coleman, Quantum sine-Gordon equation as the massive Thirring model, Phys. Rev. D **11**, 2088 (1975).

[2] L. Faddeev and V. Korepin, Quantum theory of solitons, Phys. Rep. **42**, 1 (1978).

[3] J. I. Cirac, P. Maraner, and J. K. Pachos, Cold Atom Simulation of Interacting Relativistic Quantum Field Theories, Phys. Rev. Lett. **105**, 190403 (2010).

[4] S. Samuel, Grand partition function in field theory with applications to sine-Gordon field theory, Phys. Rev. D **18**, 1916 (1978).

[5] I. Affleck and M. Oshikawa, Field-induced gap in Cu benzoate and other $s = \frac{1}{2}$ antiferromagnetic chains, Phys. Rev. B **60**, 1038 (1999).

[6] S. A. Zvyagin, A. K. Kolezhuk, J. Krzystek, and R. Feyerherm, Excitation Hierarchy of the Quantum Sine-Gordon Spin Chain in a Strong Magnetic Field, Phys. Rev. Lett. **93**, 027201 (2004).

[7] I. Umegaki, H. Tanaka, T. Ono, H. Uekusa, and H. Nojiri, Elementary excitations of the $s = \frac{1}{2}$ one-dimensional antiferromagnet $KCuGaF_6$ in a magnetic field and quantum sine-Gordon model, Phys. Rev. B **79**, 184401 (2009).

[8] F. H. L. Essler and R. M. Konik, in *From Fields to Strings: Circumnavigating Theoretical Physics* (World Scientific, 2005), p. 684.

[9] T. Giamarchi, *Quantum Physics in One Dimension* Vol. 121 (Clarendon Press, 2003).

[10] A. Roy and H. Saleur, Quantum electronic circuit simulation of generalized sine-Gordon models, Phys. Rev. B **100**, 155425 (2019).

[11] A. Roy, D. Schuricht, J. Hauschild, F. Pollmann, and H. Saleur, The quantum sine-Gordon model with quantum circuits, Nucl. Phys. B **968**, 115445 (2021).

[12] F. A. Smirnov, *Form Factors in Completely Integrable Models of Quantum Field Theory* (World Scientific, 1992).

[13] A. B. Zamolodchikov and A. B. Zamolodchikov, Factorized *S*-matrices in two dimensions as the exact solutions of certain relativistic quantum field theory models, Ann. Phys. (NY) **120**, 253 (1979).

[14] P. Calabrese, F. H. L. Essler, and G. Mussardo, Introduction to "quantum integrability in out of equilibrium systems", J. Stat. Mech.: Theory Exp. **2016**, 064001 (2016).

[15] B. Bertini, F. Heidrich-Meisner, C. Karrasch, T. Prosen, R. Steinigeweg, and M. Žnidarič, Finite-temperature transport in one-dimensional quantum lattice models, Rev. Mod. Phys. **93**, 025003 (2021).

[16] A. Bastianello, B. Bertini, B. Doyon, and R. Vasseur, Introduction to the special issue on emergent hydrodynamics in integrable many-body systems, J. Stat. Mech.: Theory Exp. **2022**, 014001 (2022).

[17] B. Bertini, D. Schuricht, and F. H. L. Essler, Quantum quench in the sine-Gordon model, J. Stat. Mech.: Theory Exp. **2014**, P10035 (2014).

[18] M. Kormos and G. Zaránd, Quantum quenches in the sine-Gordon model: A semiclassical approach, Phys. Rev. E **93**, 062101 (2016).

[19] A. C. Cubero and D. Schuricht, Quantum quench in the attractive regime of the sine-Gordon model, J. Stat. Mech.: Theory Exp. **2017**, 103106 (2017).

[20] I. Kukuljan, S. Sotiriadis, and G. Takacs, Correlation Functions of the Quantum Sine-Gordon Model in and out of Equilibrium, Phys. Rev. Lett. **121**, 110402 (2018).

[21] C. Rylands and N. Andrei, Loschmidt amplitude and work distribution in quenches of the sine-Gordon model, Phys. Rev. B **99**, 085133 (2019).

[22] B. Bertini, L. Piroli, and M. Kormos, Transport in the sine-Gordon field theory: From generalized hydrodynamics to semiclassics, Phys. Rev. B **100**, 035108 (2019).

[23] I. Kukuljan, S. Sotiriadis, and G. Takács, Out-of-horizon correlations following a quench in a relativistic quantum field theory, J. High Energy Phys. **2020**, 224 (2020).

[24] E. Wybo, M. Knap, and A. Bastianello, Quantum sine-Gordon dynamics in coupled spin chains, Phys. Rev. B **106**, 075102 (2022).

[25] V. Gritsev, A. Polkovnikov, and E. Demler, Linear response theory for a pair of coupled one-dimensional condensates of interacting atoms, Phys. Rev. B **75**, 174511 (2007).

[26] V. Gritsev, E. Demler, M. Lukin, and A. Polkovnikov, Spectroscopy of Collective Excitations in Interacting Low-Dimensional Many-Body Systems Using Quench Dynamics, Phys. Rev. Lett. **99**, 200404 (2007).

[27] T. Schweigler, V. Kasper, S. Erne, I. Mazets, B. Rauer, F. Cataldini, T. Langen, T. Gasenzer, J. Berges, and J. Schmiedmayer, Experimental characterization of a quantum many-body system via higher-order correlations, Nature **545**, 323 (2017).

[28] T. V. Zache, T. Schweigler, S. Erne, J. Schmiedmayer, and J. Berges, Extracting the Field Theory Description of a Quantum Many-Body System from Experimental Data, Phys. Rev. X **10**, 011020 (2020).

[29] M. Pigneur, T. Berrada, M. Bonneau, T. Schumm, E. Demler, and J. Schmiedmayer, Relaxation to a Phase-Locked Equilibrium State in a One-Dimensional Bosonic Josephson Junction, Phys. Rev. Lett. **120**, 173601 (2018).

[30] T. Schumm, S. Hofferberth, L. M. Andersson, S. Wildermuth, S. Groth, I. Bar-Joseph, J. Schmiedmayer, and P. Krüger, Matter-wave interferometry in a double well on an atom chip, Nat. Phys. **1**, 57 (2005).

[31] S. Hofferberth, I. Lesanovsky, B. Fischer, T. Schumm, and J. Schmiedmayer, Non-equilibrium coherence dynamics in one-dimensional Bose gases, Nature **449**, 324 (2007).

[32] T. Langen, S. Erne, R. Geiger, B. Rauer, T. Schweigler, M. Kuhnert, W. Rohringer, I. E. Mazets, T. Gasenzer, and J. Schmiedmayer, Experimental observation of a generalized Gibbs ensemble, Science **348**, 207 (2015).

[33] B. Rauer, S. Erne, T. Schweigler, F. Cataldini, M. Tajik, and J. Schmiedmayer, Recurrences in an isolated quantum many-body system, Science **360**, 307 (2018).

[34] Y. D. van Nieuwkerk, J. Schmiedmayer, and F. H. L. Essler, Projective phase measurements in one-dimensional Bose gases, SciPost Phys. **5**, 46 (2018).

[35] P. Blakie, A. Bradley, M. Davis, R. Ballagh, and C. Gardiner, Dynamics and statistical mechanics of ultra-cold Bose gases using c-field techniques, Adv. Phys. **57**, 363 (2008).

[36] A. D. Luca and G. Mussardo, Equilibration properties of classical integrable field theories, J. Stat. Mech.: Theory Exp. **2016**, 064011 (2016).

[37] A. B. Zamolodchikov, Mass scale in the sine-Gordon model and its reductions, Int. J. Mod. Phys. A **10**, 1125 (1995).

[38] L. Faddeev and L. Takhtajan, *Hamiltonian Methods in the Theory of Solitons* (Springer Science & Business Media, 2007).

[39] S. G. Chung, Thermodynamics of the Classical Massive-Thirring-Sine-Gordon Model, Phys. Rev. Lett. **62**, 708 (1989).

[40] V. Kasper, J. Marino, S. Ji, V. Gritsev, J. Schmiedmayer, and E. Demler, Simulating a quantum commensurate-incommensurate phase transition using two Raman-coupled one-dimensional condensates, Phys. Rev. B **101**, 224102 (2020).

[41] O. Chelpanova, S. P. Kelly, G. Morigi, F. Schmidt-Kaler, and J. Marino, Injection and nucleation of topological defects in the quench dynamics of the Frenkel-Kontorova model (2022), ArXiv:2210.14904.

[42] D. X. Horváth, S. Sotiriadis, M. Kormos, and G. Takács, Inhomogeneous quantum quenches in the sine-Gordon theory, SciPost Phys. **12**, 144 (2022).

[43] G. Vidal, Efficient Simulation of One-Dimensional Quantum Many-Body Systems, Phys. Rev. Lett. **93**, 040502 (2004).

[44] V. E. Korepin, N. M. Bogoliubov, and A. G. Izergin, *Quantum Inverse Scattering Method and Correlation Functions*, Vol. 3 (Cambridge University Press, 1997).

[45] C. Gross and W. S. Bakr, Quantum gas microscopy for single atom and spin detection, Nat. Phys. **17**, 1316 (2021).

[46] M. Atala, M. Aidelsburger, M. Lohse, J. T. Barreiro, B. Paredes, and I. Bloch, Observation of chiral currents with ultracold atoms in bosonic ladders, Nat. Phys. **10**, 588 (2014).

[47] A. J. Ferris and G. Vidal, Perfect sampling with unitary tensor networks, Phys. Rev. B **85**, 165146 (2012).

[48] M. Buser, U. Schollwöck, and F. Grusdt, Snapshot-based characterization of particle currents and the hall response in synthetic flux lattices, Phys. Rev. A **105**, 033303 (2022).

[49] B. Bertini, M. Collura, J. De Nardis, and M. Fagotti, Transport in Out-of-Equilibrium *XXZ* Chains: Exact Profiles of Charges and Currents, Phys. Rev. Lett. **117**, 207201 (2016).

[50] O. A. Castro-Alvaredo, B. Doyon, and T. Yoshimura, Emergent Hydrodynamics in Integrable Quantum Systems out of Equilibrium, Phys. Rev. X **6**, 041065 (2016).

[51] J. Hauschild and F. Pollmann, Efficient numerical simulations with tensor networks: Tensor Network PYTHON (TeNPy), SciPost Phys. Lect. Notes, 5 (2018), code available from https://github.com/tenpy/tenpy, ArXiv:1805.00055.

[52] E. Wybo, A. Bastianello, M. Aidelsburger, I. Bloch, and M. Knap, Preparing and analyzing solitons in the sine-Gordon model with quantum gas microscopes (2023).